Design and Applications of Solar Sail Periodic Orbits in the Non-Autonomous Earth-Moon System

Heiligers, Jeannette; Macdonald, Malcolm; Parker, Jeffrey S.

Publication date
2015

Document Version
Accepted author manuscript

Published in
AIAA/AAS Astrodynamics Specialist Conference, Vail, Colorado, USA

Citation (APA)
Heiligers, J., Macdonald, M., & Parker, J. S. (2015). Design and Applications of Solar Sail Periodic Orbits in the Non-Autonomous Earth-Moon System. In J. D. Turner, G. G. Wawrzyniak, W. T. Cerven, & M. Majji (Eds.), *AIAA/AAS Astrodynamics Specialist Conference, Vail, Colorado, USA* (Vol. 156, pp. 845-864). Article AAS 15-626

AAS 15-626

DESIGN AND APPLICATIONS OF SOLAR SAIL PERIODIC ORBITS IN THE NON-AUTONOMOUS EARTH-MOON SYSTEM

Jeannette Heiligers,[*] Malcolm Macdonald,[†] and Jeffrey S. Parker[‡]

Solar sailing has great potential for a range of high-energy and long duration missions in the Sun-Earth system. This paper extends this potential to the non-autonomous Earth-Moon system through the use of a differential correction scheme, and by selecting suitable in-plane and out-of-plane sail steering laws to develop new families of solar sail libration point orbits that are periodic with the Sun's motion around the Earth-Moon system. New orbits include those that bifurcate from the natural Lyapunov, halo and eight-shaped orbit families at the first and second Lagrange points. The potential of these orbits is demonstrated by considering the performance of a subset of orbits for high-latitude Earth observations, lunar far-side communications, and lunar South Pole coverage.

INTRODUCTION

The 21st of May 2010 saw the dawn of a new era in space propulsion when the Japanese Space Agency (JAXA) launched its IKAROS spacecraft [1]. Twenty days into the mission, IKAROS unfurled a 14 m x 14 m solar sail that would take the probe on a six-month voyage to Venus. Propelled solely by the solar photons reflecting off the 7.5 μm thin, highly reflective membrane, IKAROS was the first to demonstrate a notion that had been around for nearly a century: already in 1921, Konstantin Tsiolkovsky, the Soviet pioneer of astronautics, envisaged that spacecraft could be propelled through space by sunlight [2].

After JAXA's and other successes (e.g. NASA's 3 m x 3m NanoSail-D2 sail, 2010 [3] and The Planetary Society's 6 m x 6 m LightSail-1[§] sail, 2015), solar sailing is rapidly gaining momentum with new initiatives scheduled for the future including NASA's Lunar Flashlight[**] and NEA Scout missions [4]. Its potential lies in the fact that, contrary to other forms of propulsion, solar sails do not rely on an on-board propellant source: the Sun is the propellant source. Solar sailing can therefore be considered a breakthrough in space propulsion as it enables long-lifetime and high-energy concepts. Proposed ideas include missions over the poles of the Sun for heliophysics [5], hovering along the Sun-Earth line for space weather forecasting [6], and parking the sail above the Earth's orbit for high-latitude navigation and communication [7]. Although very promising, these concepts are all defined in the Sun-Earth system and therefore inherently far away from the Earth and unsuitable for lunar communications and/or observations.

This paper investigates the solar sail dynamics closer to the Earth, in the Earth-Moon system, allowing for new families of orbits to be defined and potentially novel applications to be enabled. Compared to the solar sail dynamics in the Sun-Earth system, the solar sail in the Earth-Moon system introduces the com-

[*] Research Associate, Advanced Space Concepts Laboratory, Department of Mechanical and Aerospace Engineering, University of Strathclyde, U.K., jeannette.heiligers@strath.ac.uk. Currently a Marie Curie Research Fellow at Faculty of Aerospace Engineering, Delft University of Technology, Kluyverweg 1, 2629 HS Delft, the Netherlands.
[†] Senior lecturer, Advanced Space Concepts Laboratory, Department of Mechanical and Aerospace Engineering, University of Strathclyde, 75 Montrose Street, Glasgow, G1 1XJ, U.K.
[‡] Assistant Professor, Colorado Center for Astrodynamics Research, University of Colorado, Boulder, CO 80309.
[§] LightSail | The Planetary Society, http://sail.planetary.org/, accessed 20 June 2015
[**] Lunar Flashlight | Solar System Exploration Research Virtual Institute, http://sservi.nasa.gov/articles/lunar-flashlight/, accessed 7 April 2015

plexity of the Sun rotating around the Earth-Moon system once per synodic lunar month, causing the direction of the photons impinging on the solar sail to change accordingly. As a result, the problem is time-dependent and the period of the orbit has to be equal to a fraction (or multiple) of the synodic lunar month in order for the orbit to be repeatable over time.

Previous work on solar sail periodic orbits in the Earth-Moon system either linearised the equations of motion [8, 9] or searched for bespoke orbits (e.g. below the lunar South Pole [10]) by solving the accompanying optimal control problem. Initial results on families of solar sail periodic orbits in the Earth-Moon system do exist [11] but have been found by solving a two-point boundary value problem, while this paper develops a faster and more accurate differential correction scheme. Furthermore, this paper extends the families found in 11 to Lyapunov and halo orbits around both the L_1 and L_2 points and introduces solar sail eight-shaped orbits. Finally, this paper investigates the performance of some of the orbits for Earth observation and lunar communication and observation applications.

The structure of the paper is as follows. First, the dynamics of the system will be introduced, followed by the derivation of the differential correction scheme used to generate families of solar sail periodic orbits. The natural Lyapunov, halo and eight-shaped orbits that serve as initial guesses for the differential corrector will subsequently be derived. After introducing three *in-plane* solar sail steering laws, the resulting families of solar sail periodic orbits will be presented. Finally, an *out-of-plane* steering strategy will be considered and some initial investigations into the application of so-called flower-shaped orbits for Earth observation, Lyapunov and eight-shaped orbits for lunar far-side communication and a constellation of eight-shaped orbits for lunar South Pole coverage will be provided.

DYNAMICAL SYSTEM

In the well-known circular restricted three-body problem (CR3BP), the motion of an object with an infinitely small mass m (here, the sailcraft) is described under the influence of the gravitational attraction of two much larger primary objects with masses m_1 (the Earth) and m_2 (the Moon). The gravitational influence of the small object on the primaries is neglected and the primaries are assumed to move in circular (co-planar) orbits about their common centre-of-mass.

Figure 1a shows the synodic reference frame that is employed in the CR3BP: the origin coincides with the centre-of-mass of the system, the x-axis connects the primaries and points in the direction of the smaller of the two, m_2, while the z-axis is directed perpendicular to the plane in which the two primaries move. The y-axis completes the right-handed reference frame. Finally, the frame rotates at constant angular velocity ω about the z-axis: $\boldsymbol{\omega} = \omega\hat{\mathbf{z}}$.

New units are introduced, see Table 1: the sum of the two larger masses is taken as the unit of mass, i.e. $m_1 + m_2 = 1$. Then, with the mass ratio $\mu = m_2/(m_1 + m_2)$, the masses of the large bodies become $m_1 = 1-\mu$ and $m_2 = \mu$. As unit of length, the distance between the main bodies is selected, and $1/\omega$ is chosen as unit of time yielding $\omega = 1$, and so one sidereal lunar month is represented by 2π.

In the synodic frame of Figure 1a, the motion of a solar sail is described, following 12, as

$$\ddot{\mathbf{r}} + 2\boldsymbol{\omega}\times\dot{\mathbf{r}} + \boldsymbol{\omega}\times(\boldsymbol{\omega}\times\mathbf{r}) = \mathbf{a}_s - \nabla V \tag{1}$$

with $\mathbf{r} = \begin{bmatrix} x & y & z \end{bmatrix}^T$ the position vector of the sail. The terms on the left-hand side are the kinematic, coriolis and centripetal accelerations, respectively, while the terms on the right-hand side are the solar sail acceleration and the gravitational acceleration exerted by the primary masses. The gravitational potential V is given by $V = -\left(\left[1-\mu\right]/r_1 + \mu/r_2\right)$ with the vectors $\mathbf{r}_1$ and $\mathbf{r}_2$ defined as $\mathbf{r}_1 = \begin{bmatrix} x+\mu & y & z \end{bmatrix}^T$ and $\mathbf{r}_2 = \begin{bmatrix} x-(1-\mu) & y & z \end{bmatrix}^T$. Following 12, the centripetal acceleration in Eq. (1) can be written as the gradient of a scalar potential function, $\Phi = -\frac{1}{2}\|\boldsymbol{\omega}\times\mathbf{r}\|^2$, and can be combined with the gravitational potential into a new, effective potential, $U = -\frac{1}{2}(x^2+y^2) - \left(\left[1-\mu\right]/r_1 + \mu/r_2\right)$. The new set of equations of motion then becomes

$$\ddot{\mathbf{r}} + 2\boldsymbol{\omega}\times\dot{\mathbf{r}} = \mathbf{a}_s - \nabla U\,. \tag{2}$$

Finally, the solar sail acceleration is described using an ideal sail model [12]. An ideal solar sail is a sail that is perfectly reflecting and perfectly flat. The incoming solar photons are therefore specularly reflected and the solar radiation pressure force acts perpendicular to the sail surface, in direction $\hat{\mathbf{n}}$. Furthermore, assuming that the solar radiation pressure is constant in magnitude throughout the Earth-Moon system, the solar sail acceleration $\mathbf{a}_s$ can be written as

$$\mathbf{a}_s = a_{0,EM}\left(\hat{\mathbf{S}}(t)\cdot\hat{\mathbf{n}}\right)^2\hat{\mathbf{n}} \ . \tag{3}$$

In Eq. (3), $\hat{\mathbf{S}}$ is the direction of the Sun-line, see Figure 1b, which can be expressed as

$$\hat{\mathbf{S}} = \begin{bmatrix}\cos(\Omega_S t) & -\sin(\Omega_S t) & 0\end{bmatrix}^T \tag{4}$$

with Ω_S the angular rate of the Sun-line in the synodic frame and in non-dimensional units, see also Table 1. Note that Eq. (4) ignores the small inclination difference between the Sun-Earth and Earth-Moon orbital planes and at time $t = 0$ the Sun is assumed to be on the negative x-axis, see also Figure 1b. Finally, note that $a_{0,EM}$ is the sail's characteristic acceleration in the non-dimensional units of the Earth-Moon CR3BP. The characteristic acceleration is the acceleration generated by the solar sail when facing the Sun at Earth's distance (at 1 astronomical unit). Derived from the previously proposed Sunjammer sail performance [6], a typical value for this characteristic acceleration is 0.215 mm/s^2, which equals a value of 0.0798 in non-dimensional units. To show what is feasible in the near-term, this paper will consider solar sail performances up to a value of $a_{0,EM} = 0.1$.

a)

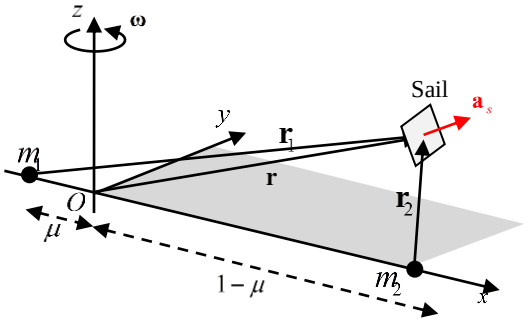

b)

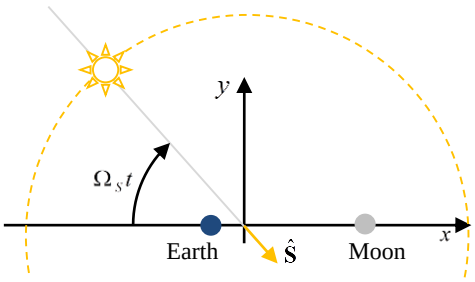

Figure 1a) Schematic of circular restricted three-body problem. b) Schematic of non-autonomous Earth-Moon three-body problem.

Table 1 Earth-Moon CR3BP parameters

μ	0.01215
Total mass ($m_1 + m_2$)	6.04718×10^{24} kg
Earth-Moon distance, λ	384,401 km
One time unit, τ	3.7749×10^{5} s
Ω_S	0.9252

DIFFERENTIAL CORRECTOR SCHEME

In order to find solar sail periodic orbits in the dynamical system described by Eq. (2), a differential corrector scheme is applied (similar to the scheme introduced in 13), which iteratively finds the initial conditions that allow for solar sail periodic orbits. The first step in deriving the differential corrector scheme is a linearisation of the equations of motion around a reference trajectory, $\mathbf{r}_0$. Replacing $\mathbf{r} \to \mathbf{r}_0 + \delta\mathbf{r}$ gives the following linearised system of first order differential equations

$$\dot{\mathbf{x}} = \mathbf{A}\mathbf{x} \tag{5}$$

with $\mathbf{x} = \begin{bmatrix}\delta\mathbf{r} & \delta\dot{\mathbf{r}}\end{bmatrix}^T$ and

$$\mathbf{A} = \begin{bmatrix} \mathbf{0} & \mathbf{I} \\ -\left.\dfrac{\partial \nabla U}{\partial \mathbf{r}}\right|_{\mathbf{r}_0} & \boldsymbol{\Omega} \end{bmatrix}, \quad \boldsymbol{\Omega} = \begin{bmatrix} 0 & 2 & 0 \\ -2 & 0 & 0 \\ 0 & 0 & 0 \end{bmatrix} . \tag{6}$$

Note that, because the solar sail acceleration is independent of the state-vector (i.e. independent of the position or velocity within the Earth-Moon system), only the partial derivative of the effective potential appears in Eq. (6). For a system of the form $\dot{\mathbf{x}} = \mathbf{A}\mathbf{x}$, as in Eq. (5), the state-vector at time t can be obtained through the state-transition matrix, $\boldsymbol{\Phi}(t;t_0)$, as

$$\mathbf{x}(t) = \boldsymbol{\Phi}(t;t_0)\mathbf{x}(t_0) \tag{7}$$

where the state transition matrix can be obtained by simultaneously integrating the equations of motion in Eq. (2) and the following differential equation for the state transition matrix

$$\dot{\boldsymbol{\Phi}}(t;t_0) = \mathbf{A}\boldsymbol{\Phi}(t;t_0) \ . \tag{8}$$

Equation (7) can be used to predict how a guess for the initial conditions needs to be changed such that the final conditions of the trajectory satisfy the requirements for a (solar sail) periodic orbit: a change in the initial conditions of $\delta\mathbf{x}(t_0)$ will change the final conditions by

$$\delta\mathbf{x}(t_f) = \boldsymbol{\Phi}(t_f;t_0)\delta\mathbf{x}(t_0) \ . \tag{9}$$

The expression in Eq. (9) is used in the following to find solar sail *halo* orbits. However, note that a similar approach can be used to find other types of periodic orbits (e.g. Lyapunov and eight-shaped orbits). Starting perpendicular to the (x,z)-plane, the initial conditions of a (solar sail) halo orbit are

$$\mathbf{x}_0 = \begin{bmatrix} x_0 & 0 & z_0 & 0 & \dot{y}_0 & 0 \end{bmatrix}^T \ . \tag{10}$$

After half the orbital period, the following final conditions should hold, which ensure that, after integration for another half period, the orbit returns to its initial conditions

$$\mathbf{x}_f = \begin{bmatrix} x_f & 0 & z_f & 0 & \dot{y}_f & 0 \end{bmatrix}^T . \tag{11}$$

However, as the first guess for the initial conditions may not be entirely correct, the final conditions will more likely be of the form

$$\tilde{\mathbf{x}}_f = \begin{bmatrix} x_f & 0 & z_f & \dot{x}_f & \dot{y}_f & \dot{z}_f \end{bmatrix}^T . \tag{12}$$

Note that the final condition $y_f = 0$ is ensured by truncating the integration of the equations of motion upon crossing the (x,z)-plane. The required change to the final conditions is thus

$$\delta\mathbf{x}_f = \begin{bmatrix} -\dot{x}_f & -\dot{z}_f \end{bmatrix}^T \tag{13}$$

which needs to be translated into a required change to the initial conditions. Using Eq. (9) does not take the variability of the final conditions with time into account (the integration time until crossing the (x,z)-plane changes when changing the initial conditions). The change in final conditions is therefore expanded with a Taylor series about the final time up to first order

$$\delta\mathbf{x}(t_f + \delta t_f) = \delta\mathbf{x}(t_f) + \left.\frac{\partial \mathbf{x}}{\partial t}\right|_{t=t_f} \delta t_f \tag{14}$$

where the first term on the right hand side can be obtained from Eq. (9), while the second term can be rewritten as

$$\delta\mathbf{x}(t_f + \delta t_f) = \boldsymbol{\Phi}(t_f;t_0)\delta\mathbf{x}(t_0) + \left.\frac{\partial \mathbf{x}}{\partial t}\right|_{t=t_f} \delta t_f \ . \tag{15}$$

Equation (15) is a system of six equations, but from Eq. (13) it is clear that only the 4th and 6th equations are of interest

$$\begin{bmatrix} -\dot{x}_f \\ -\dot{z}_f \end{bmatrix} = \begin{bmatrix} \Phi_{f,41} & \Phi_{f,43} & \Phi_{f,45} \\ \Phi_{f,61} & \Phi_{f,63} & \Phi_{f,65} \end{bmatrix} \begin{bmatrix} \delta x_0 \\ \delta z_0 \\ \delta \dot{y}_0 \end{bmatrix} + \begin{bmatrix} \ddot{x}_f \\ \ddot{z}_f \end{bmatrix} \delta t_f \,. \tag{16}$$

Note that Eq. (16) uses a short notation for $\Phi\left(t_f;t_0\right) \to \Phi_f$. The system in Eq. (16) consists of two equations with four unknowns (δx_0, δz_0, $\delta \dot{y}_0$ and δt_f). First, δt_f is used to drive the period of the orbit to a particular reference value. For the solar sail periodic orbits in the Earth-Moon system that period needs to equal the synodic lunar month, $2\pi / \Omega_S$, or a multiple thereof. The required time at the half-way point of the orbit, i.e., upon crossing the (x,z)-plane, should then equal $t_{f,req} = \pi / \Omega_S$. The value for δt_f can thus be computed as

$$\delta t_f = t_{f,req} - t_f \tag{17}$$

with t_f the actual time upon crossing the (x,z)-plane. Equation (17) reduces the number of unknowns from 4 to 3, which can be solved for through Eq. (16) and

$$\delta y_f = 0 = \Phi_{f,21}\delta x_0 + \Phi_{f,23}\delta z_0 + \Phi_{f,25}\delta \dot{y}_0 + \dot{y}_f \delta t_f \,. \tag{18}$$

Using Eq. (18) to express δx_0 as a function of δz_0 and $\delta \dot{y}_0$ gives

$$\delta x_0 = -\frac{1}{\Phi_{f,21}}\left(\Phi_{f,23}\delta z_0 + \Phi_{f,25}\delta \dot{y}_0 + \dot{y}_f \delta t_f\right). \tag{19}$$

Substituting Eq. (19) into Eq. (16) and re-writing results in

$$\begin{bmatrix} -\dot{x}_f \\ -\dot{z}_f \end{bmatrix} = \begin{bmatrix} -\frac{\Phi_{f,41}\Phi_{f,23}}{\Phi_{f,21}} + \Phi_{f,43} & -\frac{\Phi_{f,41}\Phi_{f,25}}{\Phi_{f,21}} + \Phi_{f,45} & -\frac{\Phi_{f,41}\dot{y}_f}{\Phi_{f,21}} + \ddot{x}_f \\ -\frac{\Phi_{f,61}\Phi_{f,23}}{\Phi_{f,21}} + \Phi_{f,63} & -\frac{\Phi_{f,61}\Phi_{f,25}}{\Phi_{f,21}} + \Phi_{f,65} & -\frac{\Phi_{f,61}\dot{y}_f}{\Phi_{f,21}} + \ddot{z}_f \end{bmatrix} \begin{bmatrix} \delta z_0 \\ \delta \dot{y}_0 \\ \delta t_f \end{bmatrix}. \tag{20}$$

Using the short notation

$$\begin{bmatrix} -\dot{x}_f \\ -\dot{z}_f \end{bmatrix} = \begin{bmatrix} A & B & C \\ D & E & F \end{bmatrix} \begin{bmatrix} \delta z_0 \\ \delta \dot{y}_0 \\ \delta t_f \end{bmatrix} \tag{21}$$

the system in Eq. (20) can be solved for δz_0 and $\delta \dot{y}_0$ as

$$\begin{bmatrix} \delta z_0 \\ \delta \dot{y}_0 \end{bmatrix} = -\frac{1}{BD - AE} \begin{bmatrix} -E & B & BF - CE \\ D & -A & CD - AF \end{bmatrix} \begin{bmatrix} \dot{x}_f \\ \dot{z}_f \\ \delta t_f \end{bmatrix}. \tag{22}$$

Note that once δz_0 and $\delta \dot{y}_0$ are obtained, δx_0 can be computed from Eq. (19). This approach does not require one of the three non-zero initial conditions to be fixed (as is the case for the scheme in 13). The initial condition is thus fully flexible, while driving the period of the orbit to one synodic lunar month (or a multiple thereof). Not having to fix one of the three non-zero conditions is important, because it cannot be known *a priori* for which values of x_0, z_0 or $\dot{y}_0$ solar sail periodic orbits exist.

INITIAL GUESS

To initiate the differential corrector method a suitable initial guess is required. In this paper, a continuation approach is adopted, where the search for solar sail periodic orbits starts from natural libration point orbits that have a suitable period. The sail performance in terms of characteristic acceleration $a_{0,EM}$ is then slowly increased and the solution for the previous value for $a_{0,EM}$ is used as initial guess for a slightly larger value for $a_{0,EM}$. This will give rise to families of periodic orbits for increasing sail performance.

Only natural libration point orbits with a period equal to a fraction of the synodic lunar month would be suitable initial guess candidates, i.e. the following constraint applies

$$P_{\text{Nat}} = \frac{i}{j}\frac{2\pi}{\Omega_S} \text{ with } i = 1,2,... \text{ and } j = 1,2,3... \ . \tag{23}$$

Figure 2 to Figure 4 show the families of natural Lyapunov, halo and eight-shaped orbits including their orbital periods. The orbits that fulfill the constraint in Eq. (23) are indicated with a thick blue line and a blue asterisk. For the Lyapunov orbits, see Figure 2, both selected orbits at L_1 and L_2 have period of $P_{\text{Nat Lyap}} = \pi / \Omega_S$ and thus make two orbital revolutions in one synodic lunar month. The same holds for the selected natural halo orbit at L_2, $P_{\text{Nat Halo, L}_2} = \frac{1}{2}\frac{2\pi}{\Omega_S}$, Figure 3, but the natural halo orbit at L_1 has a period of $P_{\text{Nat Halo, L}_1} = \frac{1}{3}\frac{2\pi}{\Omega_S}$ and therefore makes three orbital revolutions per synodic lunar month. Finally, for the eight-shaped orbits, see Figure 4, suitable natural orbits are found at L_1 with $P_{\text{Nat 8-shaped,L}_1} = \frac{1}{2}\frac{2\pi}{\Omega_S}$, and at L_2 with $P_{\text{Nat 8-shaped,L}_2} = \frac{2}{3}\frac{2\pi}{\Omega_S}$. The latter therefore makes three revolutions per *two* synodic lunar months.

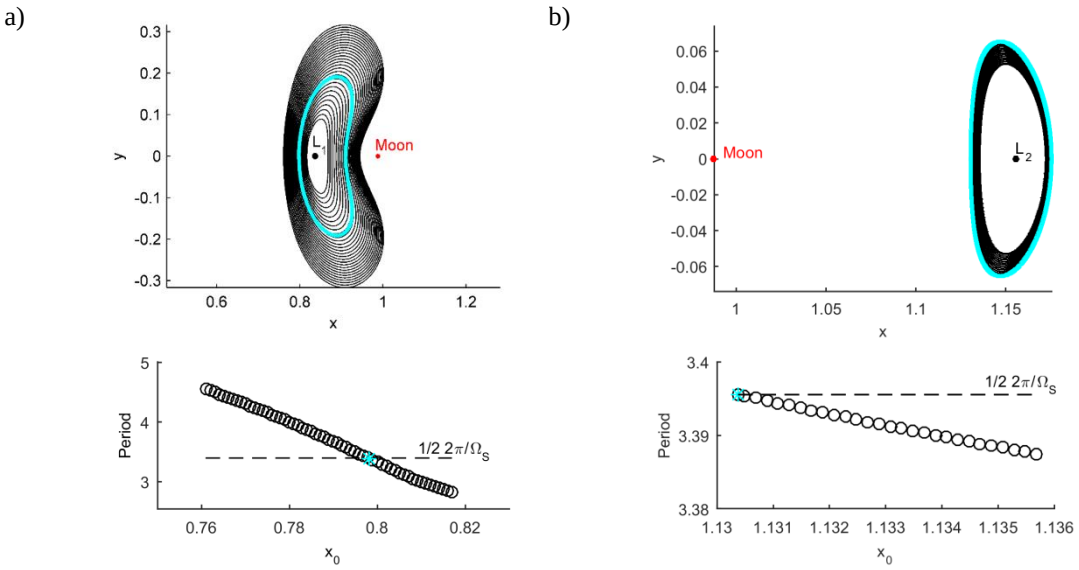

Figure 2 Families of natural Lyapunov orbits and their orbital period. a) At L_1. b) At L_2.

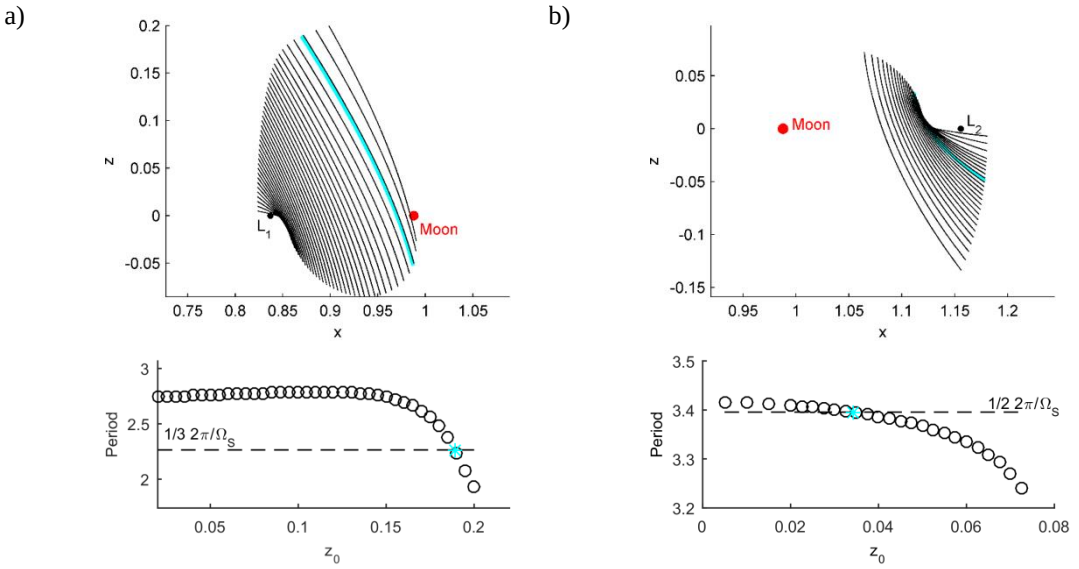

Figure 3 Families of natural halo orbits and their orbital period. a) At L_1. b) At L_2.

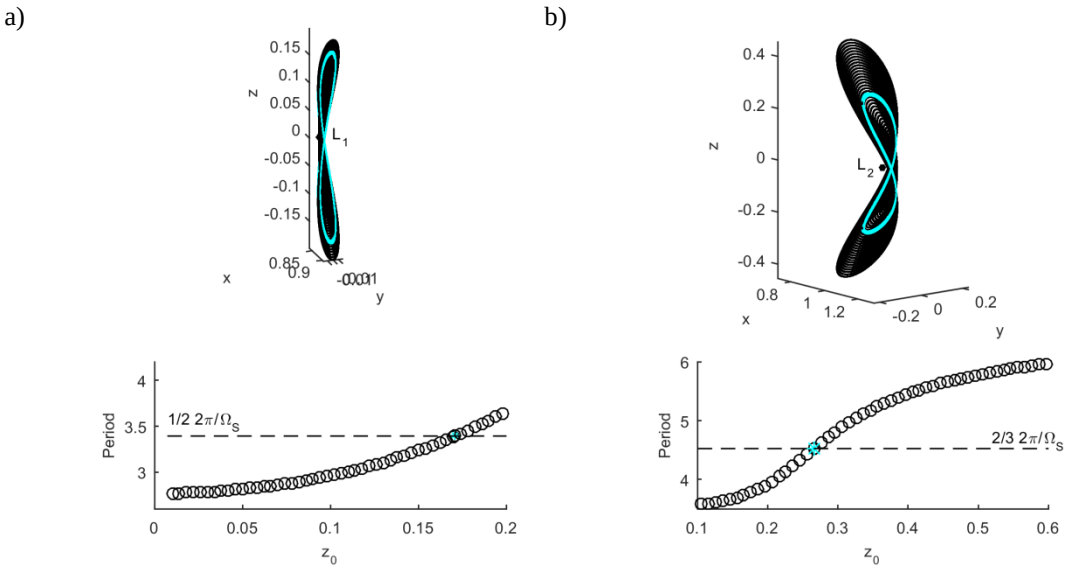

Figure 4 Family of natural eight-shaped orbits and their orbital period. a) At L_1. b) At L_2.

SOLAR SAIL STEERING LAWS

Different families of solar sail periodic orbits can be generated for different solar sail steering laws. The three laws investigated in this paper are:

1) Earth-Moon (EM) line steering law

With this steering law, the sail normal is always directed along the Earth-Moon line, i.e. along the x-axis

$$\hat{\mathbf{n}} = \text{sign}\left(\cos\left(\Omega_S t\right)\right)\begin{bmatrix}1 & 0 & 0\end{bmatrix}^T \quad . \tag{24}$$

This steering law allows for a constant attitude of the sail in the Earth-Moon synodic frame (and constant acceleration direction), but implies a changing solar sail acceleration magnitude. The term $\text{sign}\left(\cos\left(\Omega_S t\right)\right)$ takes into account that the solar sail normal vector changes sign when the Sun moves from illuminating the Earth-facing side of the sail to illuminating the Moon-facing side. Note that this implies that the sail has to be reflective on both sides, which can be achieved with a heliogyro-type sail configuration [12].

2) Constrained Earth-Moon (EM) line steering law

Conventionally, solar sails are only reflective on one side, the front side (e.g. for the first steering law, the Earth-facing side), and have a highly thermally emitting rear surface to emit the absorbed energy of the small fraction of solar radiation that, in reality, will be absorbed by the sail substrate [12]. The rear surface should therefore not be exposed to sunlight. To prevent this, a constrained Earth-Moon line steering law is defined which 'switches off' the sail by positioning the sail edge-wise to the Sun-line

$$\begin{aligned} &\hat{\mathbf{n}} = \begin{bmatrix}1 & 0 & 0\end{bmatrix}^T \quad \text{if } \left(\hat{\mathbf{S}}\cdot\hat{\mathbf{n}}\right) \geq 0 \\ &\mathbf{a}_s = \mathbf{0} \qquad\qquad \text{if } \left(\hat{\mathbf{S}}\cdot\hat{\mathbf{n}}\right) < 0, \quad \text{i.e., } \tfrac{1}{2}\pi \leq t \leq \tfrac{3}{2}\pi \end{aligned} \quad . \tag{25}$$

3) Sun-sail line steering law

With this steering law, the sail normal is always directed along the Sun-sail line, i.e. the sail always faces the Sun. Contrary to the other steering laws, this law allows for a constant magnitude of the sail acceleration ($\mathbf{a}_s = a_{0,EM}\hat{\mathbf{S}}$), but implies a changing sail acceleration direction in the synodic frame

$$\hat{\mathbf{n}} = \hat{\mathbf{S}} \quad . \tag{26}$$

Note that a Sun-facing attitude of the sail can be achieved passively [14], allowing for a very simple steering of the solar sail.

RESULTS - SOLAR SAIL LYAPUNOV ORBITS

The families of solar sail Lyapunov orbits around L_1 and L_2 for each of the steering laws described in the previous section are presented in Figure 5 and Figure 6. Figure 5 provides the initial conditions for which solar sail Lypunov orbits exist, where a cross indicates that the continuation on the solar sail acceleration failed with a minimum step size of $\Delta a_{0,EM} = 10^{-7}$. This figure shows that two different types of families are considered: those with $x_0 < x_{L_{1,2}}$ (the lower lines in Figure 5) and those with $x_0 > x_{L_{1,2}}$ (the upper lines in Figure 5). The first family, which is shown in detail in Figure 6, thus starts to the left of the L_1- or L_2-point at time $t = 0$, i.e., when the Sun is on the negative x-axis. For conciseness, the second family is only shown for the Sun-sail line steering law, see Figure 7, which starts to the right of the L_1- or L_2-point at time $t = 0$. Note that, in Figure 6 and Figure 7, the initial conditions are marked with a cross. Comparing Figure 6 and Figure 7 shows significant differences in the orbital shape as well as in the range of solar sail characteristic accelerations for which particular families exist. This shows the impact of the Sun-sail configuration at time $t = 0$ and the need for accurate injection conditions.

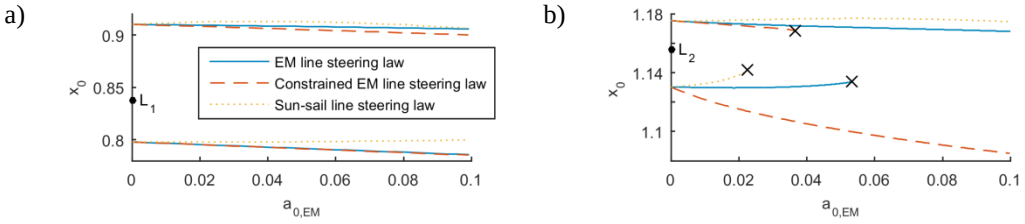

Figure 5 Initial conditions of families of solar sail Lyapunov orbits. Crosses indicate failure of the continuation with a minimum step size of $\Delta a_{0,EM} = 10^{-7}$. a) At L_1. b) At L_2.

RESULTS - SOLAR SAIL HALO ORBITS

The families of solar sail halo orbits at L_1 and L_2 for each of the three steering laws are presented in Figure 8, Figure 10 and Figure 11. Figure 8 again provides the initial conditions for which solar sail halo orbits exist. As halo orbits are three-dimensional, both the initial x- and z-coordinates are provided in Figure 8. Also the two distinct families with $x_0 < x_{L_{1,2}}$ and $x_0 > x_{L_{1,2}}$, or in case of halo orbits $z_0 > 0$ (Figure 10) and $z_0 < 0$ (Figure 11), are visible. They again show a strong dependency on the Sun-sail configuration at time $t = 0$.

For the Sun-sail line steering law at L_1 an interesting bifurcation takes place at $a_{0,EM} = 0.0241$ where the family of solar sail halo orbits transforms into a family of so-called solar sail flower-shaped orbits, see also the bottom plots in Figure 10. These orbits will later on be investigated for their application to high-latitude Earth observation. Another interesting bifurcation takes place for the family of solar sail halo orbits with a constrained Earth-Moon line steering law at L_2 and with $z_0 > 0$. At $a_{0,EM} = 0.0181$ the family of halo orbits collapses onto the family of Lyapunov orbits. This is more clearly demonstrated in Figure 9, which combines the initial conditions for the solar sail Lyapunov and halo orbits.

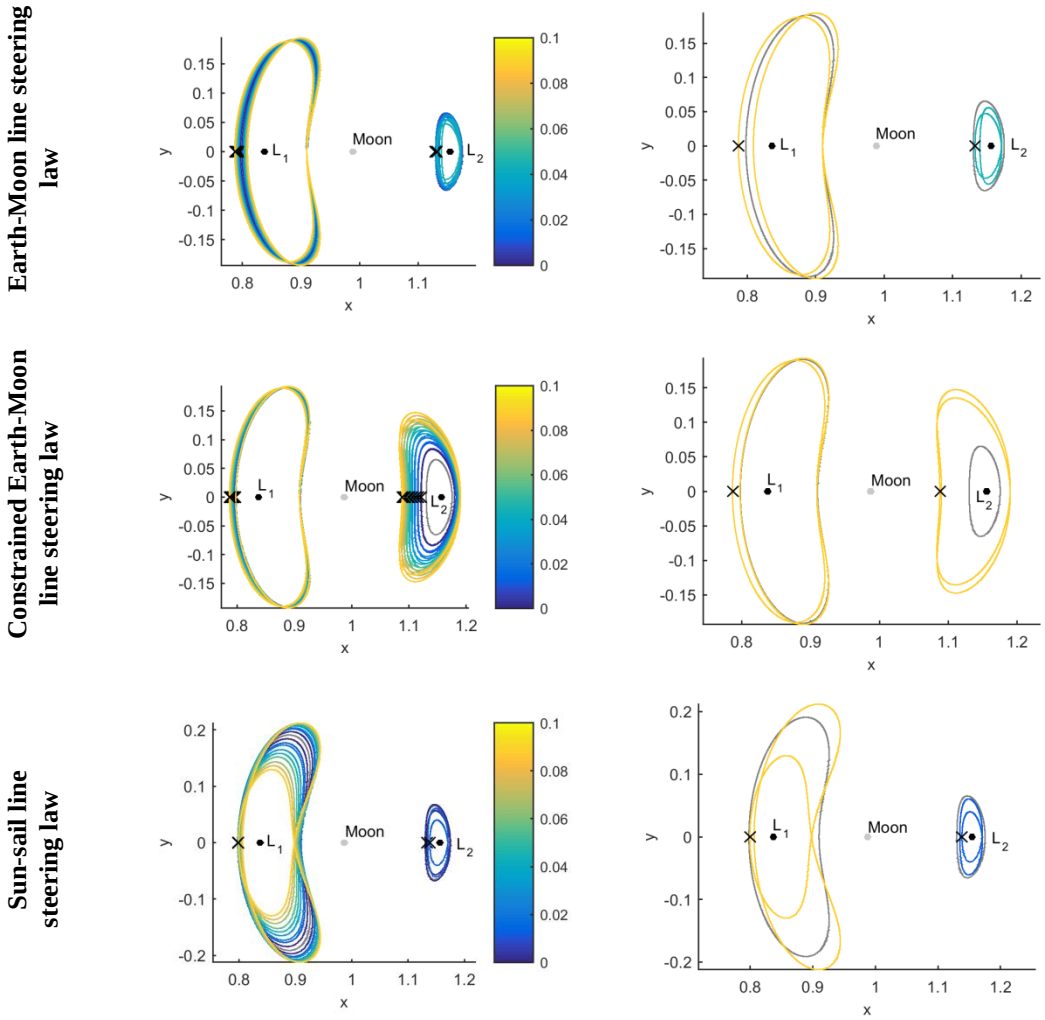

Figure 6 Solar sail Lyapunov orbits at L_1 and L_2 with $x_0 < x_{L1,2}$ at time $t = 0$ for different values for $a_{0,EM}$; grey orbit is the natural Lyapunov orbit; crosses indicate the initial condition.

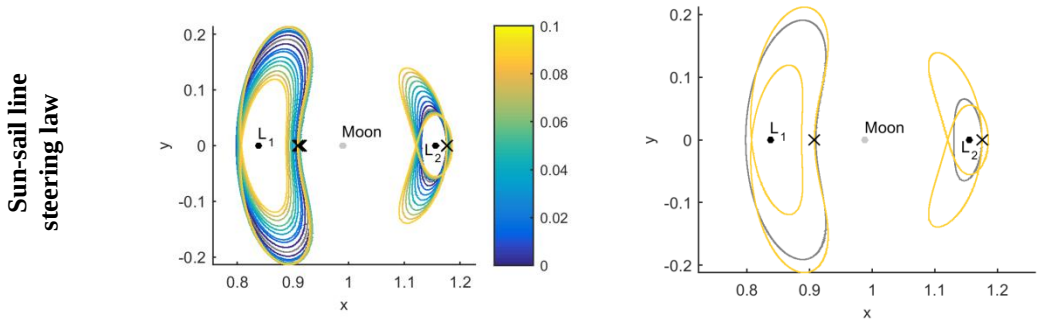

Figure 7 As Figure 6, but with $x_0 > x_{L1,2}$ at time $t = 0$.

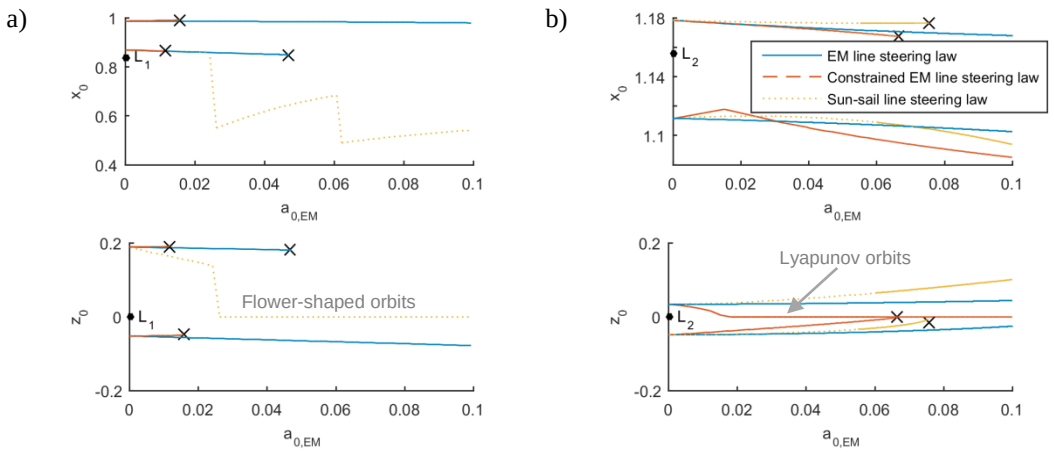

Figure 8 Initial conditions of families of solar sail halo orbits. Crosses indicate failure of the continuation with a minimum step size of $\Delta a_{0,EM} = 10^{-7}$. a) At L_1. b) At L_2.

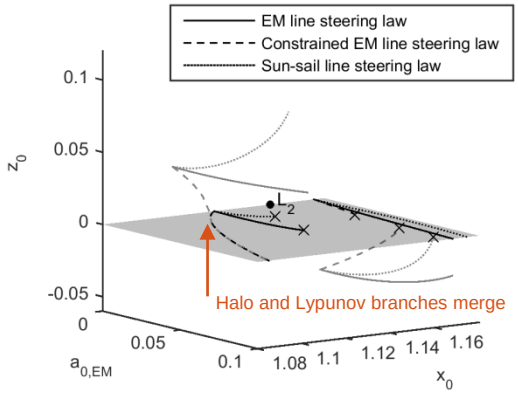

Figure 9 Initial conditions of families of solar sail Lyapunov (black) and halo (grey) orbits at L_2.

RESULTS - SOLAR SAIL EIGHT-SHAPED ORBITS

The families of solar sail eight-shaped orbits at L_1 and L_2 for each of the three steering laws are presented in Figure 12 to Figure 14. Figure 12 again provides the initial conditions for which solar sail eight-shaped orbits exist, while Figure 13 and Figure 14 provide the actual orbits at L_1 and L_2, respectively. Note that orbital plots for the case that $z_0 < 0$ are omitted as, due to symmetry, these can be obtained from mirroring the orbits for $z_0 > 0$ in the (x, y)-plane, see also Figure 12.

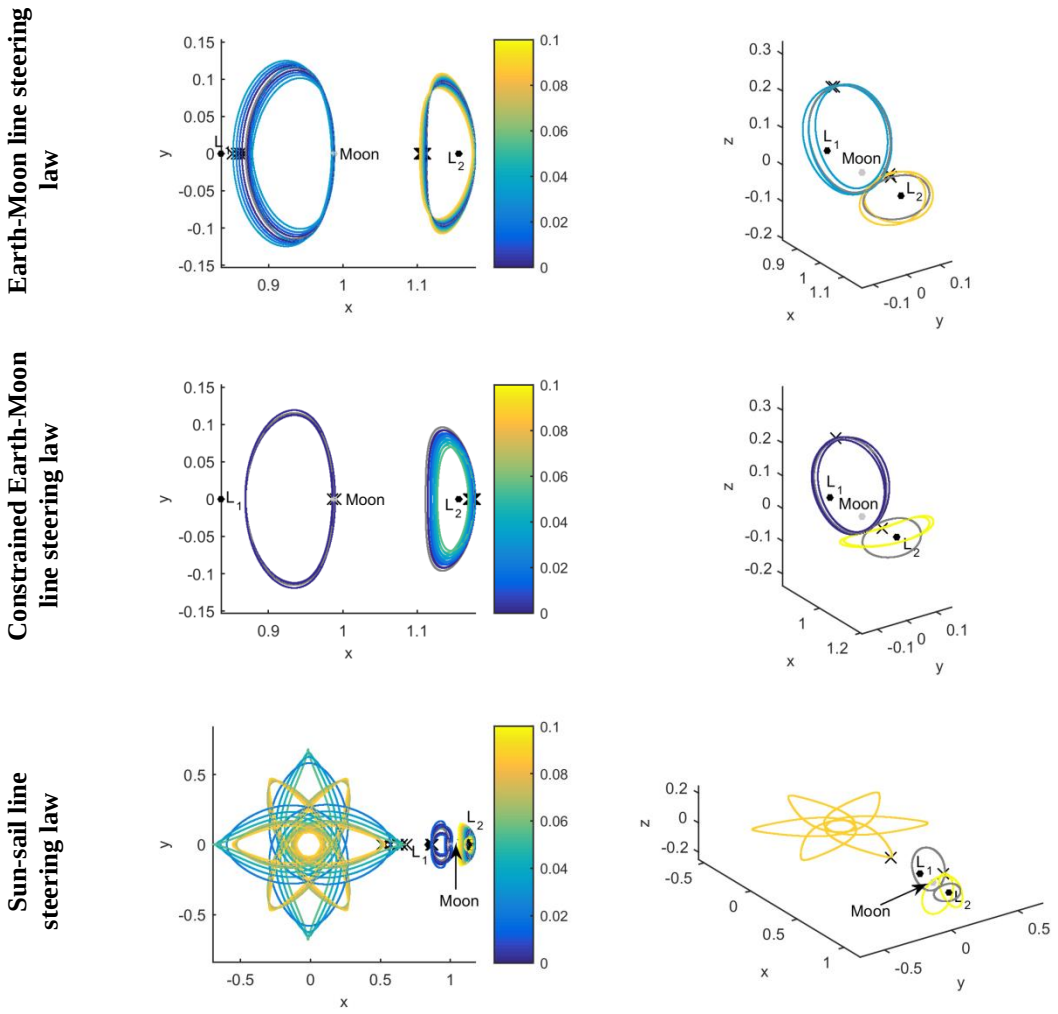

Figure 10 Solar sail periodic orbits originating from the natural halo orbits at L_1 and L_2 with $z_0 > 0$ at time $t = 0$ for different values for $a_{0,EM}$; the grey orbit is the initial natural orbit; crosses indicate the initial condition.

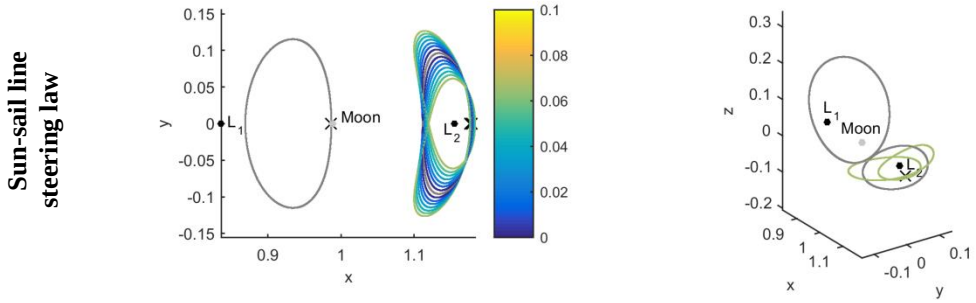

Figure 11 As Figure 10 but with $z_0 < 0$ at time $t = 0$.

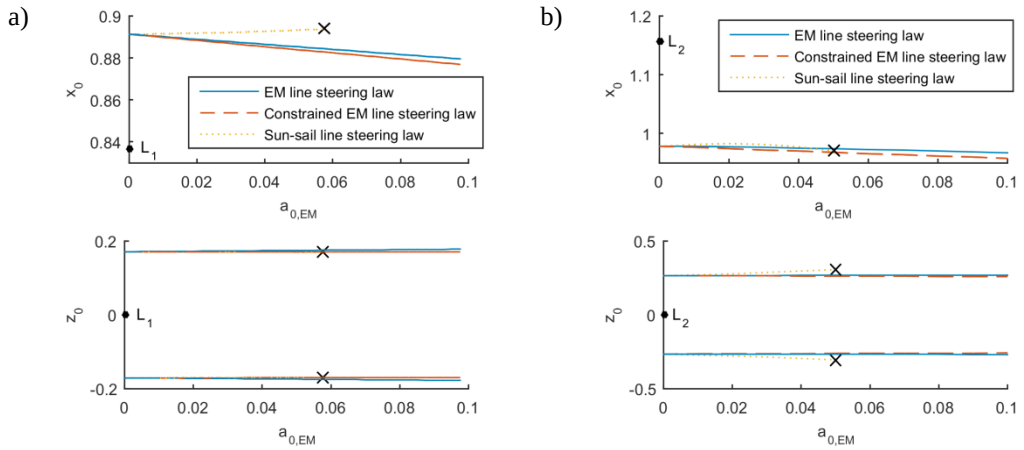

Figure 12 Initial conditions of families of solar sail eight-shaped orbits. Crosses indicate failure of the continuation with a minimum step size of $\Delta a_{0,EM} = 10^{-7}$. a) At L_1. b) At L_2.

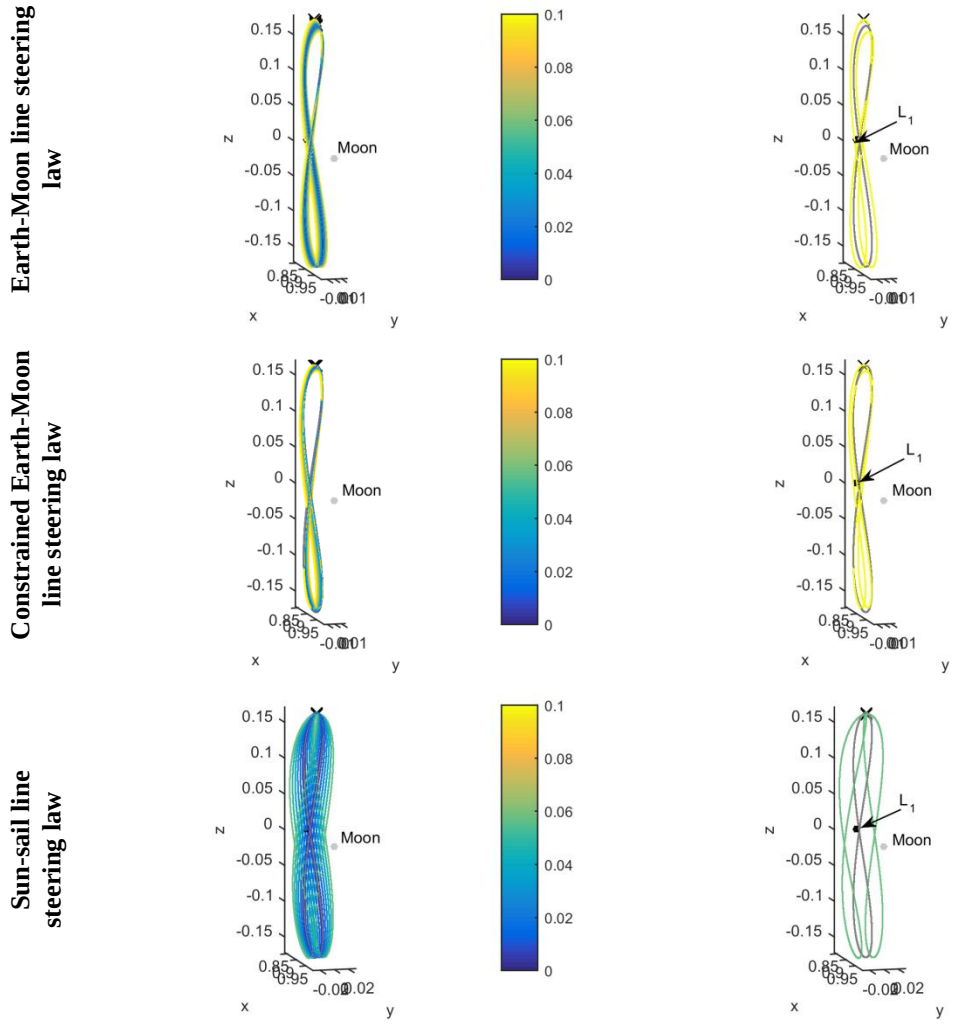

Figure 13 Solar sail periodic eight-shaped orbits at L_1 with $z_0 > 0$ at time $t = 0$ for different values for $a_{0,EM}$; grey orbit is the initial natural orbit; crosses indicate the initial condition.

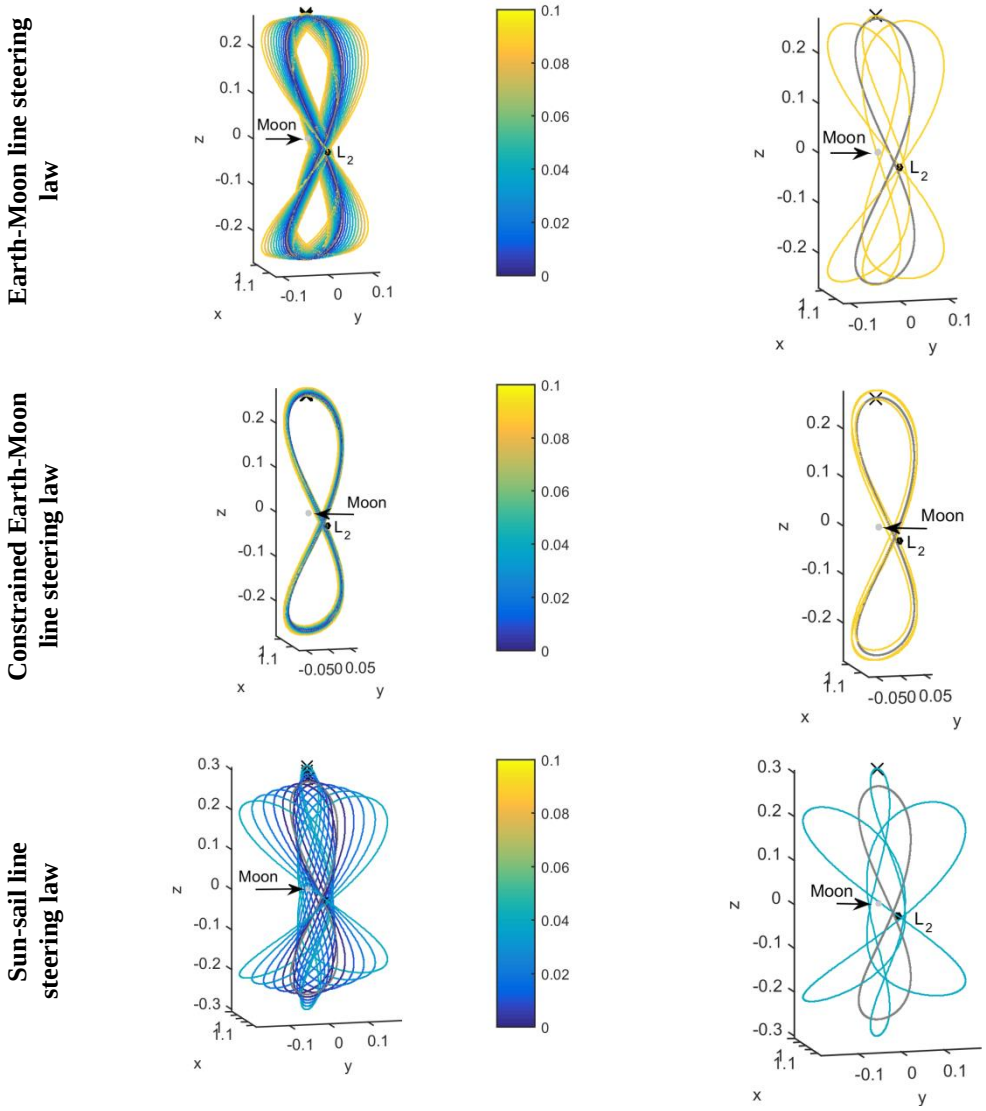

Figure 14 Solar sail periodic eight-shaped orbits at L_2 with $z_0 > 0$ at time $t = 0$ for different values for $a_{0,EM}$; grey orbit is the initial natural orbit; crosses indicate the initial condition.

OUT OF PLANE STEERING LAW

So far, the paper has only considered *in-plane* solar sail steering laws. However, by pitching the solar sail with respect to the Earth-Moon plane, an *out-of-plane* acceleration component can be created. The effect of such an out-of-plane acceleration component is investigated in this section for the Sun-sail line steering law, see Figure 15,

$$\hat{\mathbf{n}} = \begin{bmatrix} \cos\gamma\cos(\Omega_S t) & -\cos\gamma\sin(\Omega_S t) & \sin\gamma \end{bmatrix}^T . \tag{27}$$

Note that for a pitch angle $\gamma = 0$, Eq. (27) reduces to the in-plane Sun-sail line steering law in Eq. (26).

To generate families of out-of-plane periodic orbits, two different continuations can be applied:

1) A continuation on γ for a fixed value of $a_{0,EM}$:

   Starting from one of the solar sail orbits created with an in-plane steering law and for a particular value of $a_{0,EM}$, a continuation on γ can be started in which the value for $a_{0,EM}$ is kept constant.

2) A continuation on $a_{0,EM}$ for a fixed value of γ :

Starting from the natural periodic orbits, a continuation on $a_{0,EM}$ can be started using Eq. (27) with a constant value for γ as steering law.

The first type of continuation is applied to the flower-shaped orbits at L_1 of Figure 10 while the second type of continuation is applied to the family of Lyapunov orbits of Figure 6.

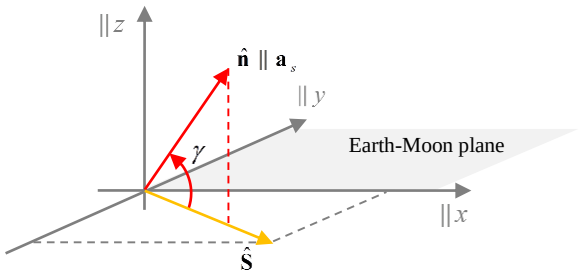

Figure 15 Schematic of out-of-plane Sun-sail line steering law

Out-of-plane flower-shaped orbits - continuation on γ for fixed value of $a_{0,EM}$

Starting from a planar solar sail flower-shaped orbit with $\gamma = 0$, out-of-plane flower-shaped orbits can be created by slowly increasing the value for the pitch angle, applying the differential corrector scheme and using the result as an initial guess for a slightly larger value for γ. The families of orbits that result from this continuation are provided in Figure 16 for three values of $a_{0,EM}$. The figures clearly show that, the larger the solar sail acceleration, the larger the out-of-plane displacement. As flower-shaped orbits do not exist beyond a value of $a_{0,EM} = 0.1222$, larger out-of-plane displacements than the ones shown in Figure 16c are not expected.

Figure 16d shows the maximum out-of-plane displacement along the orbit for the range of out-of-plane steering angles considered. For each value of $a_{0,EM}$ a clear optimum value for γ exists for which the out-of-plane displacement is maximised. Those orbits are highlighted with a thick colored line in Figure 16a-c. Note that for negative values of the pitch angle γ similar orbits, but mirrored in the (x, y)-plane, can be obtained. These orbits will later on be investigated for their application to high-latitude Earth observation.

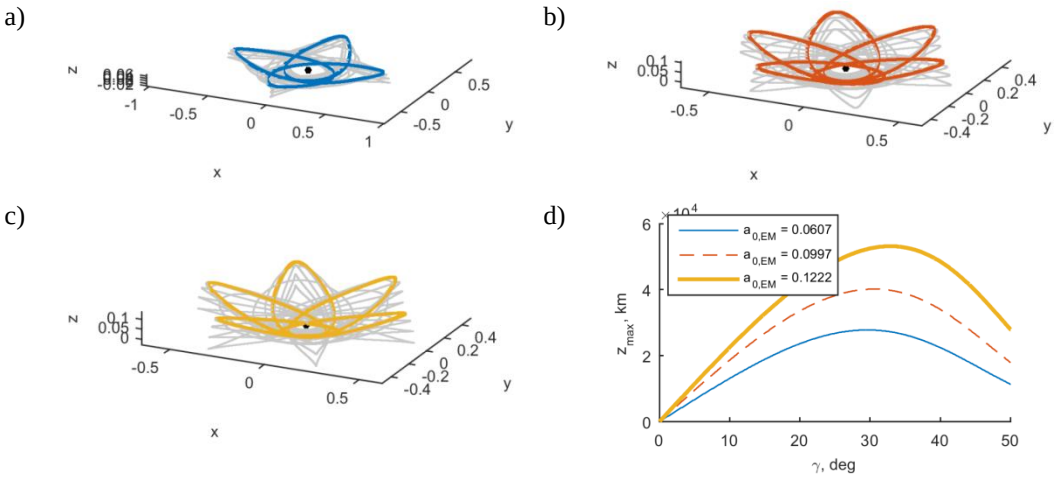

Figure 16 Out-of-plane solar sail flower-shaped orbits

Out-of-plane Lyapunov orbits - Continuation on $a_{0,EM}$ for fixed value of γ

The search for families of out-of-plane Lyapunov orbits is similar to the search for in-plane Lyapunov orbits and starts from the natural Lyapunov orbits at L_1 or L_2. The sail performance in terms of characteristic acceleration $a_{0,EM}$ is slowly increased, only now, the steering law in Eq. (27) is applied for a constant value of γ. In this section, a value of $\gamma = \pm 35.26$ deg is applied as this is known to give the maximum out-of-plane solar sail acceleration component [12].

The results are presented in Figure 17 for the case that $x_0 < x_{L_{1,2}}$ and show that a significant out-of-plane motion can be achieved even though the continuation on $a_{0,EM}$ truncates at relatively low values for $a_{0,EM}$ for the family at L_2. Note again that, for positive values of the pitch angle γ, similar orbits, but mirrored in the (x, y)-plane, can be obtained. These families of out-of-plane Lyapunov orbits will be considered in the next section for their application to lunar far-side communication.

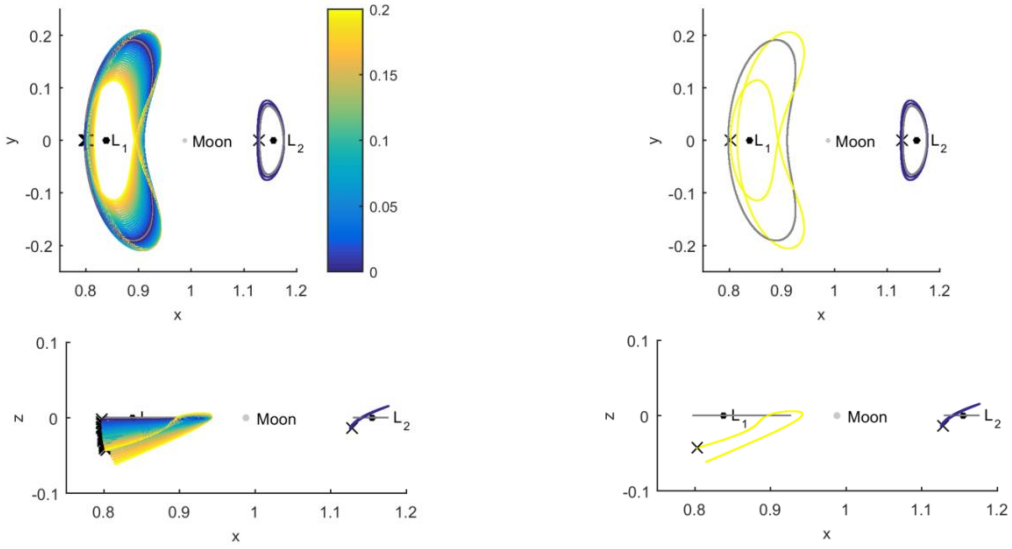

Figure 17 Out-of-plane solar sail Lyapunov orbits at L_1 and L_2 for γ = -35.26 deg, with $x_0 < x_{L1,2}$ at time t = 0 and for different values for $a_{0,EM}$; grey orbit is the initial natural orbit; crosses indicate the initial condition.

APPLICATIONS

To demonstrate the potential of the solar sail periodic orbits presented throughout this paper, this section will investigate applications of a subset of those orbits. In particular, preliminary analyses for the applications of high-latitude Earth observation, lunar far-side communication and lunar South Pole observation will be provided.

High-latitude Earth observation

Observation of the high-latitudes of the Earth is crucial to answer key questions concerning global climate change, but also to support telecommunications, weather forecasting and ship navigation for the exploration of these areas that are expected to hold 30 percent of the world's undiscovered gas and 13 percent of the world's undiscovered oil [15]. A further increase in shipping activity can be expected from the fact that the northern sea routes are opening up, allowing a fast and economic passage between the Atlantic and Pacific Oceans [16].

Observation of the high-latitudes of the Earth can be achieved with satellites in low-altitude, high-inclination orbits such as NASA's ICESat-1 mission (2003- 2010) [20] and ESA's Cryosat-2 mission (2010 – ongoing) [21]. Although enabling high spatial resolution observations, the low-altitude of the polar orbits restricts spacecraft to observe only narrow swaths of the polar regions during each passage. For example,

CryoSat repeats it ground track only after 369 days, with a sub-cycle of 33 days, only after which uniform coverage of the polar regions is obtained. Higher temporal resolution can be achieved from Molniya orbits, but satisfactory coverage of the polar caps or high-latitude regions cannot always be achieved.

In addition to these traditional concepts, the literature shows a range of other concepts for high-latitude observation, including Taranis orbits [17], pole-sitter orbits [18], and solar sail displaced equilibria [7] and eight-shaped orbits [19] in the Sun-Earth system.

To assess the potential of the out-of-plane flower-shaped orbits for high-latitude observation, the motion of the Earth's polar axis needs to be described in the synodic frame. For this, the small inclination difference between the Earth-Moon and Sun-Earth orbital planes is once again neglected. When considering the obliquity of the ecliptic, δ_{eq}, and the fact that the Earth's polar axis is inertially fixed, it becomes clear that over time the polar axis describes a cone in the synodic reference frame as shown in Figure 18a. As the angular rate of the Sun in the synodic reference frame is smaller than that of the Earth-Moon system, the Sun/polar axis configuration drifts slightly during the year, see Figure 18b. A mathematical expression for the Earth's north (subscript '*N*') and south (subscript '*S*') polar axes can be derived as

$$\begin{aligned}\mathbf{r}_N &= \left[-\mu + \sin\left(\delta_{eq}\right)\cos\left(\omega t\right) \quad -\sin\left(\delta_{eq}\right)\sin\left(\omega t\right) \quad \cos\left(\delta_{eq}\right)\right]^T \\ \mathbf{r}_S &= \left[-\mu - \sin\left(\delta_{eq}\right)\cos\left(\omega t\right) \quad \sin\left(\delta_{eq}\right)\sin\left(\omega t\right) \quad -\cos\left(\delta_{eq}\right)\right]^T\end{aligned} . \tag{28}$$

The potential of the out-of-plane flower-shaped orbits can subsequently be determined by investigating the elevation, ε, of the sail seen from an observer on the North (or equivalently South) Pole

$$\varepsilon = \tfrac{1}{2}\pi - \cos^{-1}\left(\mathbf{r}_{NP,1}\cdot\mathbf{r}_{NP\to s}\right) \tag{29}$$

$$\mathbf{r}_{NP,1} = \frac{r_E}{\lambda}\left(\mathbf{r}_N + \left[\mu \quad 0 \quad 0\right]^T\right), \quad \mathbf{r}_1 = \mathbf{r}_1 - \left[\mu \quad 0 \quad 0\right]^T, \quad \mathbf{r}_{NP\to s} = \mathbf{r}_1 - \mathbf{r}_{NP,1} \tag{30}$$

with r_E = 6378.16 km the Earth's radius and λ the Earth-Moon distance, see Table 1.

The resulting elevation as well as the sail-Pole distance of the out-of-plane flower-shaped orbit with $a_{0,EM}$ =0.1222 and γ = 32.9 deg (i.e., the colored orbit in Figure 16c) is provided in Figure 19a. The dashed black lines in the top plot represent minimum elevation angles of 10, 20 and 27 deg. The latter is included as this is the elevation of a GEO spacecraft seen from 55 deg latitude and is the maximum latitude that is conventionally considered accessible from GEO [18]. Figure 19b translates plot a) into the number of useful observation days per year at any longitude and latitude of the Earth. It shows that, for a minimum elevation angle of 10 deg, the North Pole can be observed for 163 days, i.e., 45% of the time.

Some useful observation time is lost due to the Earth's own rotation (especially for lower latitudes), while for the North Pole most observation time is lost due to the fact that the period of the flower-shaped orbit is larger than the Earth-Moon orbit period. This causes a precession of the orbit in an inertial frame and as the polar axis is inertially fixed, the orbit moves away from the direction of the polar axis, leading to a loss in observations during summer.

a) b)

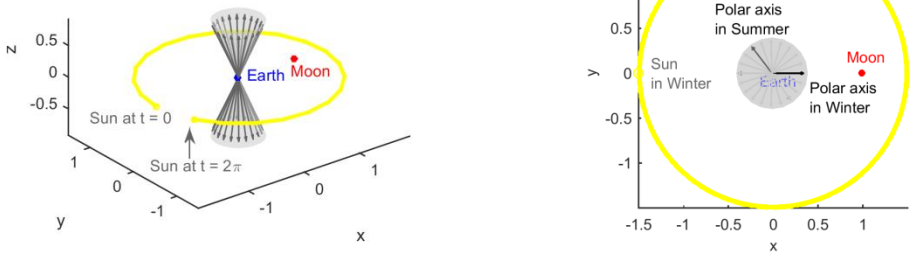

Figure 18 Polar axis in the Earth-Moon synodic reference frame

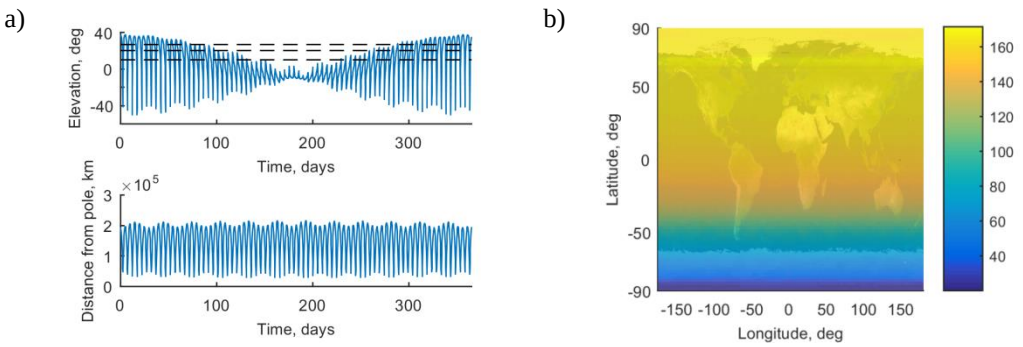

Figure 19 Out-of-plane flower-shaped orbit with $a_{0,EM}$ = 0.1222, γ = 32.9 deg a) Elevation and distance from North Pole with t = 0 at winter solstice. b) Number of useful observation days per year for a minimum elevation of 10 deg.

Some observation time can be retrieved from using a second flower-shaped orbit mirrored in the (x, y)-plane, see Figure 20. Figure 20b shows that the constellation ensures an almost uniform coverage of the Earth of between 160 and 177 useful observation days per year with good observation of the North and South Poles in winter and summer, respectively.

A full quantitative comparison between the performance of the out-of-plane flower-shaped orbits and other existing and proposed mission concepts for high-latitude Earth observation requires more detailed analyses. Here, only a qualitative analysis will be provided, where it can be concluded that the flower-shaped orbits appear to provide a midway between a constellation of LEO satellites and a pole-sitter spacecraft. For the same number of spacecraft, the flower-shaped orbits provide a much better temporal resolution than LEO satellites but half the temporal resolution of a pole-sitter spacecraft. However, in terms of spatial resolution, the flower-shaped orbits are an order of magnitude closer to the Earth than the pole-sitter concept, but are much farther from the Earth than LEO satellites. Finally, because the out-of-plane flower-shaped orbits are enabled using a solar sail only, they have benefits over concepts that are only enabled by using low-thrust propulsion technologies that rely on a finite propellant source (e.g. electric propulsion).

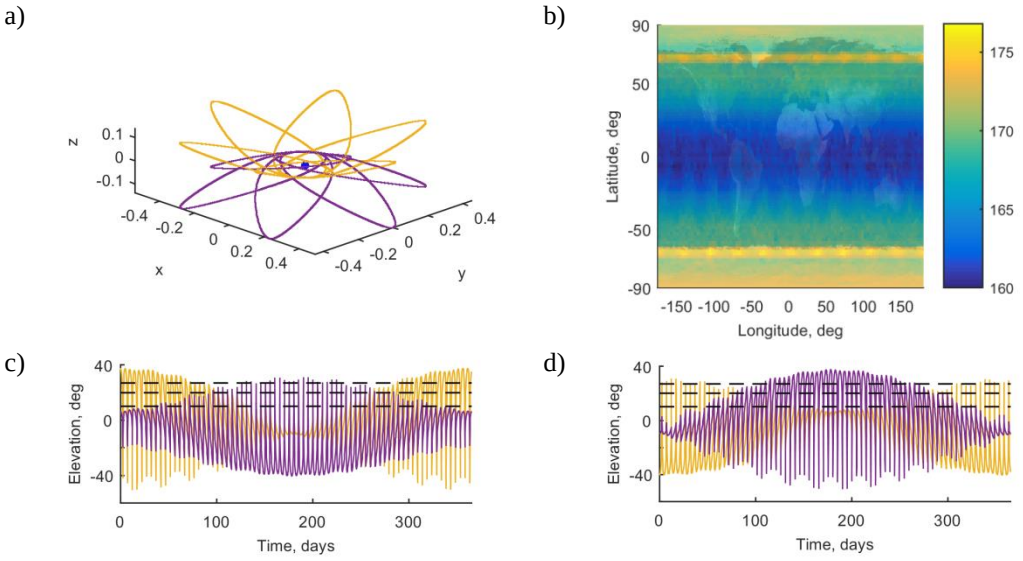

Figure 20 Constellation of mirrored out-of-plane flower-shaped orbits with $a_{0,EM}$ = 0.1222, γ = 32.9 deg. a) Orbits. b) Number of useful observation days per year for a minimum elevation of 10 deg. c-d) Elevation at North (c) and South (d) Pole with t = 0 at winter solstice.

Lunar far-side communications

For future (human) exploration of the Moon, a continuous communication link with the far-side of the Moon will be essential. Traditionally, natural halo orbits at L_2 are proposed to this end [20, 21] because they allow a direct line-of-sight with both the far-side of the Moon and the Earth. Natural Lyapunov and eight-shaped orbits are discarded because part of the orbit is inherently occulted by the Moon. However, as Figure 17 showed, Lyapunov orbits *can* be lifted out of the Earth-Moon plane using a solar sail acceleration, removing the occultation. This is also clear from the (y,z)-projections in Figure 21a of the L_2-orbit of Figure 17 and its counterpart in Figure 21b for $x_0 > x_{L_2}$. With the Moon depicted at its true size, it is clear that these out-of-plane solar sail Lyapunov orbits, which have become similar to halo orbits, allow a continuous communication link between the Earth and the far-side of the Moon.

Applying the same out-of-plane continuation scheme to the natural eight-shaped orbit at L_2, the family of out-of-plane solar sail eight-shaped orbits of Figure 22 can be created. The figure clearly shows that the solar sail acceleration moves the cross point of the figure of eight away from the Earth-Moon line, thereby again removing the occultation.

To assess how well the out-of-plane Lyapunov and eight-shaped orbits perform for lunar far-side communication compared to natural halo orbits depends on orbital properties such as the distance to the Earth and Moon (for power requirements), the distance to the Earth-Moon line (for tracking purposes) and stability properties, which will all be part of future analyses. The main purpose of this section has been to demonstrate that adding a solar sail opens up the possibility of using Lyapunov and eight-shaped orbits for lunar far-side communication purposes.

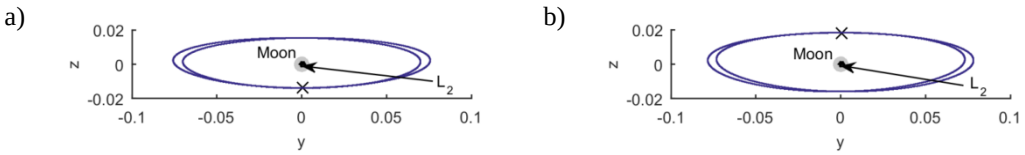

Figure 21 (y,z)-projection of out-of-plane solar sail Lyapunov orbits at L_2 for $a_{0,EM}$ = 0.01 and γ = -35.26 deg. The Moon is depicted at its true size. a) $x_0 < x_{L2}$ at time t = 0. b) $x_0 > x_{L2}$ at time t = 0.

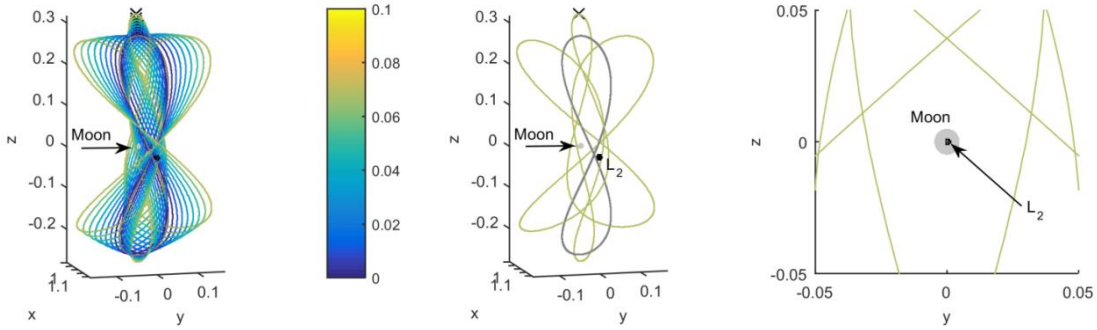

Figure 22 Out-of-plane solar sail eight-shaped orbits at L_2 for γ = 35.26 deg, with $z_0 > 0$ at time t = 0 and for different values for $a_{0,EM}$; grey orbit is the initial natural orbit; crosses indicate the initial condition. The Moon is depicted at its true size.

Lunar South Pole coverage

Due to its permanently shadowed craters and the potential presence of valuable resources, the lunar South Pole is of great scientific interest and is also regarded as a potential destination for a permanent lunar base. Both objectives require a continuous observation and/or communications link with the lunar South Pole. The literature lists a range of concepts that could achieve this link, including a low-altitude constellation around the Moon, a set of satellites in natural Lagrange point orbits [22], and a single solar sail craft in an optimal lunar South Pole orbit [10].

While the work in 22 indicated that a constellation of two natural eight-shaped orbits cannot achieve the required continuous link with the South Pole as the satellites will simultaneously be at the x-axis cross point, Figure 22 already indicated that this cross point can be displaced away from the Earth-Moon line. Exploiting this feature and considering two out-of-plane solar sail eight-shaped orbits with γ = -35.26 deg (one with $z_0 > 0$ and one with $z_0 < 0$), the constellation as depicted in Figure 23a can be achieved. The sailcrafts' elevation above the South Pole is shown in Figure 23b which is computed by once again assuming that the Earth-Moon plane and ecliptic plane coincide and that the very small inclination of the lunar spin axis with respect to the ecliptic of 1.5 deg can be neglected. Then, the spin axis of the Moon is parallel to the z-axis of the synodic reference frame. Furthermore, Figure 23b includes a minimum elevation of 15 deg in compliance with the work in 10 and 22. It is clear that the constellation of Figure 23a meets this minimum elevation as well as enabling large elevation angles for prolonged periods of time, which is advantageous for maintaining line-of-sight with infrastructure in craters.

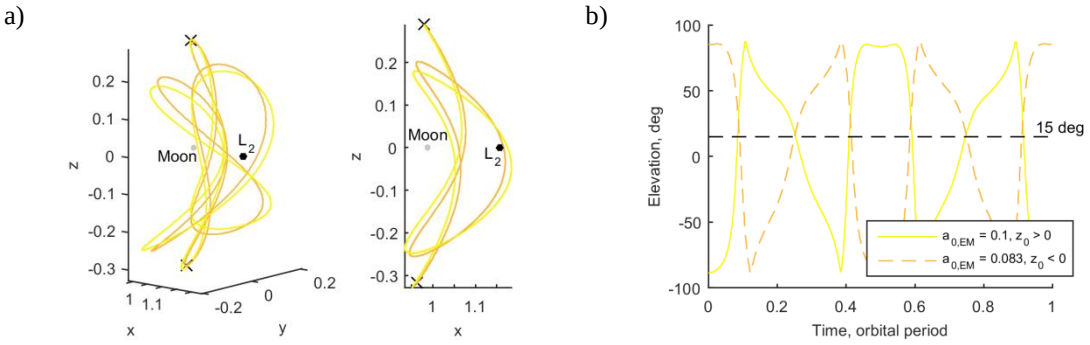

Figure 23 Constellation of out-of-plane solar sail eight-shaped orbits at L_2 with γ = -35.26 deg; crosses indicate the initial condition. a) Constellation. b) Elevation at lunar South Pole.

As mentioned for the other two applications, a thorough evaluation of the performance of this constellation requires a comparison with other proposed concepts. Compared to a constellation of low-orbiting satellites, the solar sail eight-shaped orbit constellation requires fewer satellites to establish a continuous view, while it requires more satellites than the single South Pole-sitter sailcraft proposed in 10. However, instead of a relatively complex control law that requires continuous steering of the solar sail, the solar sail eight-shaped orbit constellation requires only a simple (and potentially passive) Sun-pointing steering law. However, more comparisons, for example in terms of distance to the South Pole (again, for power requirements), need to be considered to draw solid conclusions on the performance compared to other orbit constellations for lunar South Pole coverage. In any case, this section once again demonstrates that the use of a solar sail opens up opportunities that are not available within the classical Earth-Moon system.

CONCLUSIONS

This paper has introduced new families of solar sail periodic orbits in the non-autonomous Earth-Moon system, bifurcating from the natural Lyapunov, halo and eight-shaped orbits at the L_1 and L_2 points. These orbits have been found using a new differential corrector scheme and applying a continuation on the solar sail characteristic acceleration. All families are commensurate with the period of the Sun around the Earth-Moon system and often exist up to large values of the solar sail characteristic acceleration. Families have been generated for a range of *in-plane* solar sail steering laws that employ either a constant direction of the sail acceleration or a constant sail acceleration magnitude. The latter, which is achieved with a simple and potentially passive Sun-facing sail attitude, produces the greatest offset between the natural and solar sail libration point orbits. Finally, two different initial Sun-sail configurations have been considered, resulting in completely different families and therefore indicating the need for accurate orbit injection conditions.

Subsequently, by applying an *out-of-plane* solar sail steering law, even more families of solar sail periodic orbits have been generated. Bifurcating from the family of halo orbits, a set of out-of-plane solar sail flower-shaped orbits centered at the Earth have been investigated for high-latitude observation of the Earth, where two sailcraft have been shown to achieve full coverage of the Earth approximately 50% of the time. Furthermore, out-of-plane solar sail Lyapunov and eight-shaped orbits have been created, opening up pos-

sibilities to use these types of orbits for lunar far-side communication, something that natural Lyapunov and eight-shaped orbits do not allow due to their occultation by the Moon. Finally, similar out-of-plane solar sail eight-shaped orbits have been shown to possess great potential for continuous lunar South Pole coverage. This is again contrary to their natural counterparts, which again shows how solar sails can open up opportunities that are not available within the classical Earth-Moon system.

ACKNOWLEDGMENTS

This work was funded by a John Moyes Lessells Travel Scholarship of the Royal Society of Edinburgh and by the Marie Skłodowska-Curie Individual Fellowship 658645 - S4ILS: Solar Sailing for Space Situational Awareness in the Lunar System.

REFERENCES

1. Tsuda, Y., Mori, O., Funase, R., Sawada, H., Yamamoto, T., Saiki, T., Endo, T., Yonekura, K., Hoshino, H., and Kawahuchi, J. "Achievement of IKAROS - Japanese deep space solar sail demonstration mission," *Acta Astronautica* Vol. 82, 2013, pp. 183-188.doi: 10.1016/j.actaastro.2012.03.032
2. Tsiolkovsky, K. E. "Extension of Man into Outer Space." 1921.
3. Johnson, L., Whorton, M., Heaton, A., Pinson, R., Laue, G., and Adams, C. "NanoSail-D: A Solar Sail Demonstration Mission," *Acta Astronautica* Vol. 68, 2011, pp. 571-575.doi: 10.1016/j.actaastro.2010.02.008
4. McNutt, L., Johnson, L., Clardy, D., Castillo-Rogez, J., Frick, A., and Jones, L. "Near-Earth Asteroid Scout," *AIAA SPACE 2014 Conference and Exposition*. American Institute of Aeronautics and Astronautics, San Diego, CA, 2014.
5. Macdonald, M., Hughes, G. W., McInnes, C. R., Lyngvi, A., Falkner, P., and Atzei, A. "Solar Polar Orbiter: A Solar Sail Technology Reference Study," *Journal of Spacecraft and Rockets* Vol. 43, No. 5, 2006, pp. 960-972.doi: 10.2514/1.16408
6. Heiligers, J., Diedrich, B., Derbes, B., and McInnes, C. R. "Sunjammer: Preliminary End-to-End Mission Design," *2014 AIAA/AAS Astrodynamics Specialist Conference*. San Diego, CA, USA, 2014.
7. Waters, T. J., and McInnes, C. R. "Periodic Orbits Above the Ecliptic in the Solar-Sail Restricted Three-Body Problem," *Journal of Guidance, Control, and Dynamics* Vol. 30, No. 3, 2007, pp. 687-693.doi: 10.2514/1.26232
8. McInnes, C. R. "Solar Sail Trajectories at the Lunar L2 Lagrange Point," *Journal of Spacecraft and Rockets* Vol. 30, No. 6, 1993, pp. 782-784.doi: 10.2514/3.26393
9. Simo, J., and McInnes, C. R. "Solar Sail Orbits at the Earth-Moon Libration Points," *Communications in Nonlinear Science and Numerical Simulation* Vol. 14, No. 12, 2009, pp. 4191-4196.doi: 10.1016/j.cnsns.2009.03.032
10. Wawrzyniak, G. G., and Howell, K. C. "Generating Solar Sail Trajectories in the Earth-Moon System Using Augmented Finite-Difference Methods (Article ID 476197)," *International Journal of Aerospace Engineering*, 2011.doi: 10.1155/2011/476197
11. Heiligers, J., Hiddink, S., Noomen, R., and McInnes, C. R. "Solar Sail Periodic Orbits in the Earth-Moon Three-Body Problem," *65th International Astronautical Congress*. Toronto, Canada, 2014.
12. McInnes, C. R. *Solar Sailing: Technology, Dynamics and Mission Applications*. Berlin: Springer-Praxis Books in Astronautical Engineering, Springer-Verlag, 1999.
13. Howell, K. C. "Three-Dimensional, Periodic, 'Halo' Orbits," *Celestial Mechanics and Dynamical Astronomy* Vol. 32, 1983, pp. 53-71.doi: 10.1007/BF01358403
14. Atchison, J. A., and Peck, M. A. "A Passive, Sun-Pointing, Millimeter-scale Solar Sail," *Acta Astronautica* Vol. 67, No. 1-2, 2010, pp. 108-121.doi: 10.1016/j.actaastro.2009.12.008
15. Gautier, D. L., Bird, K. J., Charpentier, R. R., Grantz, A., Houseknecht, D. W., Klett, T. R., Moore, T. E., Pitman, J. K., Schenk, C. J., Schuenemeyer, J. H., Sørensen, K., Tennyson, M. E., Valin, Z. C., and C.J., W. "Assessment of Undiscovered Oil and Gas in the Arctic," *Science* Vol. 324, No. 5931, 2009, pp. 1175-1179.doi: 10.1126/science.1169467
16. Johannessen, O. M., Alexandrov, V. Y., Frolov, I. Y., Sandven, S., Pettersson, L. H., VBobylev, L. P., Kloster, K., Smirnov, V. G., Mironov, Y. U., and Babich, N. G. *Remote Sensing of Sea Ice in the Northern Sea Route - Studies and Applications*. Chichester, UK: Praxis Publishing Ltd, 2007.
17. Anderson, P. and Macdonald, M. "Extension of highly elliptical Earth orbits using continuous low-thrust propulsion," *Journal of Guidance, Control and Dynamics*, Vol. 36, No. 1. pp. 282-292. doi: 10.2514/1.55304
18. Ceriotti, M., Heiligers, J., and McInnes, C. R. "Trajectory and Spacecraft Design for a Pole-Sitter Mission," *Journal of Spacecraft and Rockets* Vol. 51, No. 1, 2014, pp. 311-326.doi: 10.2514/1.A32477
19. Ceriotti, M., and McInnes, C. "Natural and sail-displaced doubly-symmetric Lagrange point orbits for polar coverage," *Celestial Mechanics and Dynamical Astronomy*, 2012.doi: 10.1007/s10569-012-9422-2
20. Farquhar, R. W. "The Utilization of Halo Orbits in Advanced Lunar Operations, NASA TN D-6365," *NASA Technical Note*. Washington, D.C., 1971.
21. Farquhar, R. W. "A Halo-Orbit Lunar Station," *Astronautics & Aeronautics*, 1972, pp. 59-63
22. Grebow, D. J., Ozimek, M. T., and Howell, K. C. "Multibody Orbit Architectures for Lunar South Pole Coverage," *Journal of Spacecraft and Rockets* Vol. 45, No. 2, 2008, pp. 344-358.doi: 10.2514/1.28738